JOURNAL OF SYNCHROTRON RADIATION

ISSN 1600-5775

Received 14 January 2015
Accepted 22 June 2015

Edited by M. Yamamoto, RIKEN SPring-8 Center, Japan

Keywords: windowless ion chamber; soft X-ray beamline; gas phase absorption; dynamic beam size monitor.

A plug-and-measure diagnostic tool for flux, resolution and beam size of a soft X-ray beamline

Ching-Hsuan Wei,[a] Hong-Cheu Lin,[a]* Shang-Wei Lin[b] and Jih-Young Yuh[b]*

[a]Department of Material Science and Engineering, National Chiao Tung University, Hsinchu 30013, Taiwan, and [b]National Synchrotron Radiation Research Center, 101 Hsin-Ann Road, Hsinchu Science Park, Hsinchu 30076, Taiwan. *Correspondence e-mail: linhc@mail.nctu.edu.tw, jyyuh@nsrrc.org.tw

A compact multi-functional diagnostic tool has been installed for commissioning beamlines at the Taiwan Light Source. For a photon beam, the instrument can measure the photon flux, energy resolution and beam size, consecutively with a photodiode or gold mesh, a windowless gas cell and a movable fluorescence screen viewport. Two gratings with ruling densities of 350 and 1000 lines mm^{-1} and dispersing photons of energies from 80 to 1200 eV were calibrated with a photon flux of 10^{11} photon s^{-1} at slit openings of 50 µm × 50 µm; a maximum resolving power of greater than 10000 was certified with an absorption spectra of gaseous samples. Pressure differences over four orders of magnitude were achieved between the ion chamber and the flux measurement chamber with a single capillary differential pumping stage. A sequence of beam profiles was measured by moving continuously in the vicinity of the nominal focal positions. This tool is useful in commissioning or trouble-shooting at most beamlines in a synchrotron facility.

1. Introduction

The Taiwan Light Source is a 3 GeV storage ring operating at 360 mA in a top-up mode. The average up time of the machine is over 98% annually (Luo *et al.*, 2007); after prolonged operation during routinely scheduled beam time, carbon contamination (Boller *et al.*, 1983; Chauvet *et al.*, 2011) or misalignment of optical elements (mirrors, gratings) is unavoidable, so a quick test of the beamline performance is regularly necessary. The most important parameters such as flux, resolution, alignment and size of the beam spot (focal position) must be fine-tuned using devices such as a photodiode or gold mesh, an ion chamber, a laser and a fluorescence screen, which are generally installed separately at various sections of the beamline. Some of these tools dedicated to beamline diagnostics have recently been developed to test the beam quality and sample alignment (Muro *et al.*, 2009; Yuh, 2014), but none of those devices were integrated to measure the beamline parameters at the same time – above all, to dynamically monitor the beam quality (shape, focal position) along the beam path. We have implemented such a compact yet easily installed beamline diagnostic tool equipped with a flux detector, a windowless gas cell and a movable fluorescence screen viewport to characterize the beam quality simultaneously. The tool was applied to a newly built monochromator at beamline 08B that contains two gratings, with ruling densities of 350 and 1000 lines mm^{-1}, to disperse photons of energy from 80 to 1200 eV with a measuring flux of 1×10^{11} photon s^{-1} and a resolving power greater than 10000. The variation in the size of the beam spots could be observed and was recorded in real time with a digital microscope. The

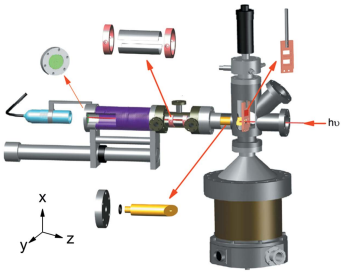

focal point and the size of the beam spot by design can thus be verified.

2. Apparatus and measurements

The design (see Fig. 1*a*) comprises three major parts: a flux chamber, an ion chamber and an imaging chamber. The photon beam from the right side enters a multiport flux-measuring chamber [70 mm OD, (a)]; inside the chamber the sample holder (h) (ceramic or Teflon) is connected to a linear-motion feedthrough. On adjusting the feedthrough up and down, two measuring devices are selected: a photodiode (IRD XUV100) at the upper position and a gold mesh at the lower position. The beam passes through the capillary (b) into the ion chamber; absorption by a gas generates the photoionization currents measured and recorded with a current meter. The photon beam is eventually dumped onto a fluorescence screen viewport (f) at the end of the retractable welded bellows (d), which generated a bright spot on the screen. On adjusting the length of the bellows, the beam profile at various positions is sectioned and a sequence of images is recorded with a digital microscope. A photograph of the system is displayed for comparison in Fig. 1(*b*); the system is installed on a pumping cart. For our tests, using a turbomolecular pump (450 l s^{-1}) a pressure of 10^{-7} torr within 2–3 h was attained. Baking was optional, but cycles of flushing the system with dry nitrogen were essential. The installation was completed within 1 h after the experimental endstation of the user was removed. A transmission mode (without removing the endstation) is practical under the following conditions: the length of the working space for the system should exceed 600 mm with the fluorescence screen removed and the flux can be measured only with a highly transmitting gold mesh.

An ion chamber is widely used to determine the absolute intensity of extreme ultraviolet light (Samson, 1964) and in photon absorption spectra experiments (Ho, 1998), in particular, to verify the total instrumental resolution of the beamline (Domke *et al.*, 1992; Chung *et al.*, 1995; Song *et al.*, 2006). Fig. 1(*a*) shows the structure of a modified ion chamber (c) decreased in size; it consists of a standard nipple (70 mm OD, length 100 cm) and three flange ports (34 mm OD). In its interior are two curved electrode plates (g) to collect the photoionization currents with a potential difference supplied at 40 V. The back-fill pressure in the ion chamber is 7–18 mtorr. A pressure difference between the ion chamber (10^{-3} torr) and the flux measurement chamber (10^{-7} torr) was achieved by isolating with a capillary (diameter 1 mm, length 80 mm), which was optimized to diminish the conductance of the gas flow. To visualize the variation of the spot size in the x–y plane, a fluorescence screen moved continuously in the z direction with a retractable stage (102 mm) made of a welded bellows. The fluorescence screen viewport (70 mm OD) was uniformly coated with CdSe (material with a small work function), which, when struck with the intense beam of light from the synchrotron, clearly displayed the beam profile on the screen which was captured with a digital microscope from the atmosphere side. The spatial resolution at the image plane was defined with a CMOS detector (2 Mpixel, 2.55 mm × 1.9 mm); the pixel size is estimated to be less than 10 µm, which is sufficient for sampling a beam of size on the millimeter scale. The translational resolution along the beamline axis (z) is within 1 mm through manual adjustment, but can be improved with a stepping motor.

3. Results

The photocurrents of the photodiode were converted to a flux density on normalization of the storage ring current (360 mA) and the curve of quantum efficiency of the photodiode. Fig. 2 shows the flux of photon energy measured with two gratings; the maximum flux densities at 170 and 700 eV reached 6 × 10^{11} and 8 × 10^{10} photon s^{-1}, respectively. Two pronounced

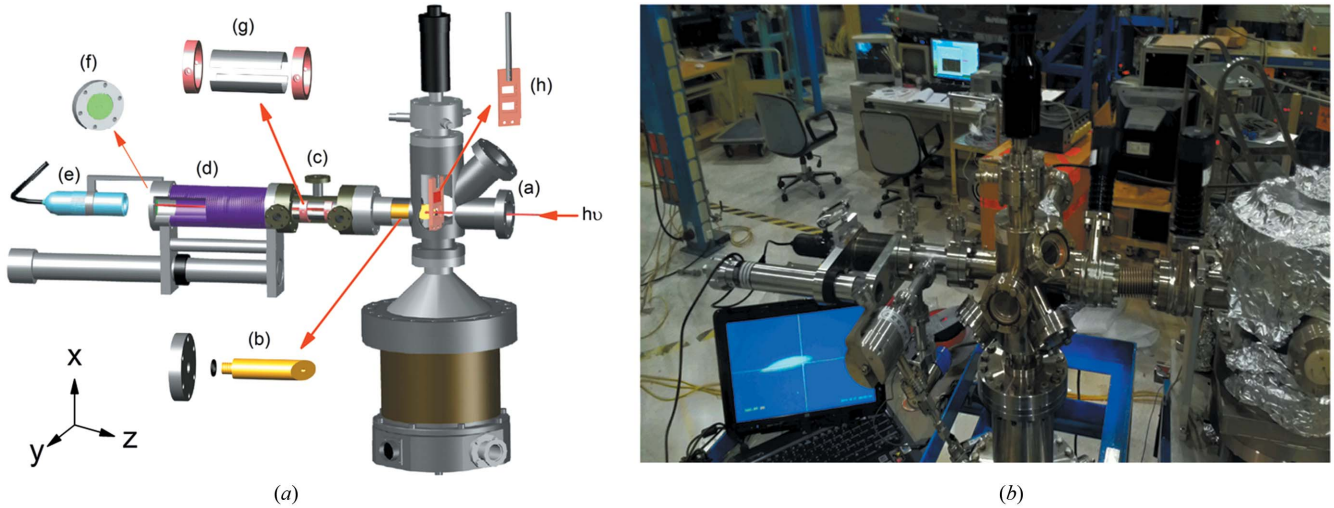

(*a*) (*b*)

Figure 1
(*a*) Assembly drawing of the beamline diagnostic tool: (a) flux measurement chamber, (b) differential capillary, (c) ion chamber, (d) retractable chamber, (e) digital microscope, (f) fluorescence viewport, (g) electrode plates and (h) photodiode holder. (*b*) Photograph of the diagnostic tool connected to BL08B.

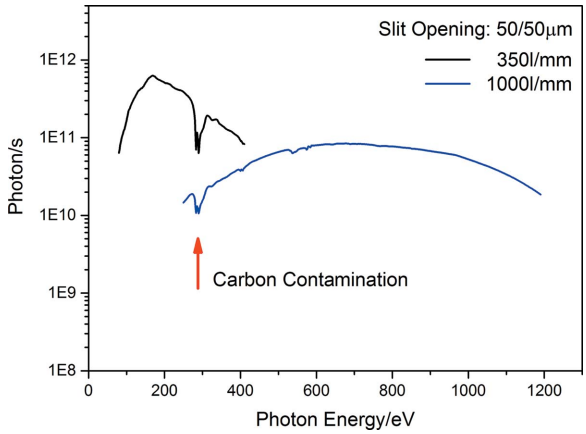

Figure 2
Flux measurement of two gratings.

absorption dips near 270 and 540 eV arose from the strong absorption of carbon and oxide contamination of the optical surfaces. The range covering from 80 to 420 eV and from 250 to 1200 eV was tested with four gases, Kr, CO, N_2 and Ne, for an analysis of the line width and energy calibration. Here, only the absorption spectrum of the nitrogen *K*-edge is presented. The spectrum in Fig. 3 was fitted with seven Voigt functions for the line of best fit after subtraction of a linear background. The Lorentzian and Gaussian widths represent the core lifetime broadening and the total instrumental resolution (slit opening, slope error, aberration and misalignment). The best-fitted widths of the first vibrational state are 127.6 meV and 38 meV for Lorentzian and Gaussian shapes, respectively. By definition, the resolving power ($E/\Delta E$) of the monochromator is greater than 10000, which is comparable with the results reported by Domke *et al.* (1992) and Prince *et al.* (1999). To verify the focal position, we sectioned the beam spot in the *x*–*y* plane with a continuously moving screen along the *z* axis. Fig. 4(*a*) shows nine snapshots, captured with a digital microscope, of the beam profile at 400 eV in the vicinity of the nominal focal point. An analysis of their detailed beam profiles (grey scale of each pixel) with a Gaussian fit in the

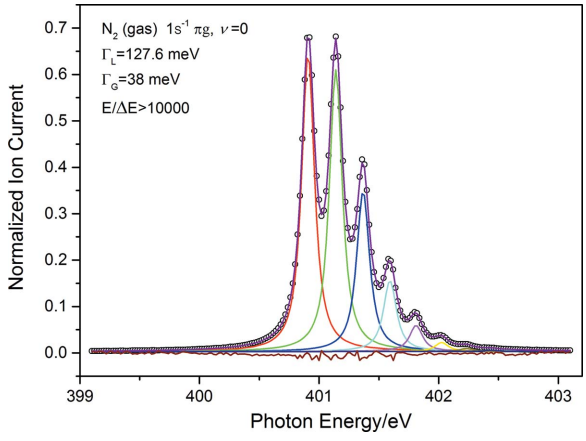

Figure 3
Vibrational progression in the absorption spectrum of nitrogen for the transition 1*s* to π^* fitted with seven lines of Voigt fit after subtraction of a linear background.

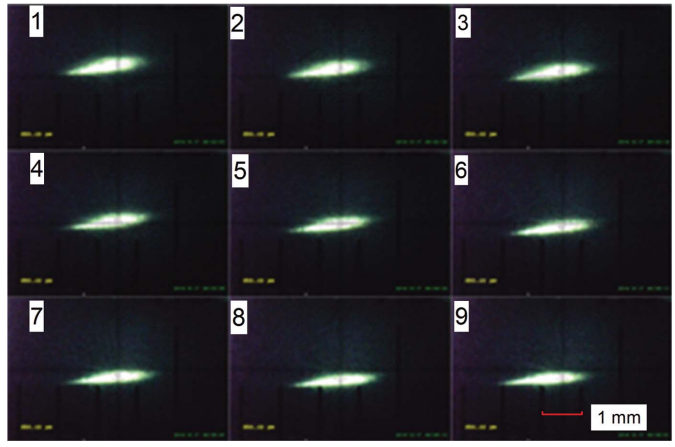

(*a*)

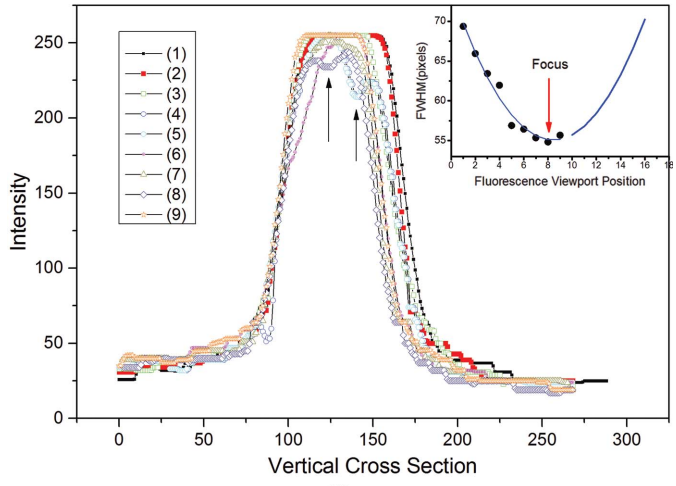

(*b*)

Figure 4
(*a*) Dynamic monitoring of the beam quality by varying the viewport position continuously. (*b*) A detailed analysis of the beam profile shows the best focus at position 8.

vertical direction (*y* direction) is shown in the inset of Fig. 4(*b*). The beam spot at the focal point has a vertical dimension of 0.55 mm and a horizontal dimension of 2.0 mm with both slits set at 50 μm.

4. Discussion

For maintaining a beamline, this tool is useful both for commissioning a new beamline and after restoration of the optical components (grating, mirror). There is no point yet in installing this tool permanently in each beamline; its highly mobile design and ease of operation should be the major benefits. Compared with our early designs (Chung *et al.*, 1995; Song *et al.*, 2006), the mass of the new ion chamber is greatly decreased from 10 kg to 0.5 kg and the length from 28 cm to 13 cm; these features facilitate the easy installation. The most challenging task was to pass the synchrotron beam through the tiny holes of the capillary; this problem was solved with the aid of a fluorescent material coated on the wedge surfaces of the capillary. In the analysis of the beam profile in Fig. 4(*b*), there

are sudden decreases of intensity (indicated with arrows) that were caused by the blurred (horizontal) lines [Fig. 4(*a*)]. These millimeter-scale rulings attached from the atmosphere side caused a shadowing effect on the digital microscope. In contrast, the intensity truncation in Fig. 4(*b*) is due to the saturation of the CMOS sensor struck by the intense beam from the synchrotron (the detector was blinded). The gradually decreasing beam profile is attributed to the slow converging power of the refocusing mirror; there is an uneven number of data points at the right side of the inset in Fig. 4(*b*) as the presumed focal position is not in the middle of the translation range of the bellows. The position of the focal point is, nevertheless, indicated by the minimum of the fitting curve. When this tool is applied for a smaller beam such as from an undulator beamline, the magnification of the microscope should be increased.

In conclusion, we have developed a compact beamline diagnostic tool that combines the abilities to measure the photon flux, resolving power and spot size in real time. The small width of the lines in the vibrational structure in the absorption spectrum of the nitrogen transition 1*s* to π^* indicates that our system is capable of enabling gas-phase experiments for beamline diagnostic purposes. The installation is easy and saves space; it might also be beneficial for applications outside the synchrotron community with having a lamp in vacuum and a small divergence.

References

Boller, K., Haelbich, R.-P., Hogrefe, H., Jark, W. & Kunz, C. (1983). *Nucl. Instrum. Methods Phys. Res.* **208**, 273–279.

Chauvet, C., Polack, F., Silly, M. G., Lagarde, B., Thomasset, M., Kubsky, S., Duval, J. P., Risterucci, P., Pilette, B., Yao, I., Bergeard, N. & Sirotti, F. (2011). *J. Synchrotron Rad.* **18**, 761–764.

Chung, S.-C., Chen, C.-I., Tseng, P.-C., Lin, H.-F., Dann, T.-E., Song, Y.-F., Huang, L.-R., Chen, C.-C., Chuang, J.-M., Tsang, K.-L. & Chang, C.-N. (1995). *Rev. Sci. Instrum.* **66**, 1655–1657.

Domke, M., Mandel, T., Puschmann, A., Xue, C., Shirley, D. A., Kaindl, G., Petersen, H. & Kuske, P. (1992). *Rev. Sci. Instrum.* **63**, 80–89.

Ho, G. H. (1998). *Chem. Phys.* **226**, 101–111.

Luo, G. H. *et al.* (2007). *AIP Conf. Proc.* **879**, 13–16.

Muro, T., Kato, Y., Kinoshita, T. & Watanabe, Y. (2009). *J. Synchrotron Rad.* **16**, 595–596.

Prince, K. C., Vondráček, M., Karvonen, J., Coreno, M., Camilloni, R., Avaldi, L. & de Simone, M. (1999). *J. Electron Spectrosc. Relat. Phenom.* **101–103**, 141–147.

Samson, J. A. R. (1964). *J. Opt. Soc. Am.* **54**, 6–15.

Song, Y. F., Yuh, J.-Y., Lee, Y.-Y., Chung, S. C., Huang, L. R., Tsuei, K.-D., Perng, S. Y., Lin, T. F., Fung, H. S., Ma, C.-I., Chen, C. T. & Tsang, K. L. (2006). *Rev. Sci. Instrum.* **77**, 085102.

Yuh, J.-Y. (2014). *J. Synchrotron Rad.* **21**, 1213–1214.